Vibrational Distributions of the CO(v) Products of the C_2H_2 + O(^{3}P) and HCCO + O(^{3}P) Reactions Studied by FTIR Emission

Viktor Chikan and Stephen. R. Leone*

Departments of Chemistry and Physics and Lawrence Berkeley National Laboratory, University of California, Berkeley, California 94720-1460

Received: August 27, 2004

The C_2H_2 + O(^{3}P) and HCCO + O(^{3}P) reactions are investigated using Fourier transform infrared (FTIR) emission spectroscopy. The O(^{3}P) radicals are produced by 193 nm photolysis of an SO_2 precursor or microwave discharge in O_2. The HCCO radical is either formed in the first step of the C_2H_2 + O(^{3}P) reaction or by 193 nm photodissociation of ethyl ethynyl ether. Vibrationally excited CO and CO_2 products are observed. The microwave discharge experiment [C_2H_2 + O(^{3}P)] shows a bimodal distribution of the CO(v) product, which is due to the sequential C_2H_2 + O(^{3}P) and HCCO + O(^{3}P) reactions. The vibrational distribution of CO(v) from the HCCO + O(^{3}P) reaction also shows its own bimodal shape. The vibrational distribution of CO(v) from C_2H_2 + O(^{3}P) can be characterized by a Boltzmann plot with a vibrational temperature of ∼2400 ± 100 K, in agreement with previous results. The CO distribution from the HCCO + O(^{3}P) reaction, when studied under conditions to minimize other processes, shows very little contamination from other reactions, and the distribution can be characterized by a linear combination of Boltzmann plots with two vibrational temperatures: 2320 ± 40 and 10 300 ± 600 K. From the experimental results and previous theoretical work, the bimodal CO(v) distribution for the HCCO + O(^{3}P) reaction suggests a sequential dissociation process of the HC(O)CO‡ → CO + HCO; HCO → H + CO.

Introduction

The oxidation of acetylene has great importance in combustion chemistry[1,2] and in processes of certain planetary atmospheres. Acetylene is easily formed in fuel rich hydrocarbon flames, and a detailed understanding of acetylene oxidation is essential for this chemistry. The first step in the combustion of acetylene is the reaction with O(^{3}P) atoms. This reaction is a slow process resulting in triplet methylene radicals and ketenyl radicals in the following pathways:

$$C_2H_2 + O(^3P) \rightarrow CH_2(^3B_1) + CO \quad (-47 \text{ kcal/mol}; -197 \text{ kJ/mol}) \quad \text{(R1a)}$$

$$\rightarrow HCCO + H \quad (-19 \text{ kcal/mol}; -80 \text{ kJ/mol}) \quad \text{(R1b)}$$

There has been a question about the relative importance of the ketenyl-producing step, although it is now well-established that R1b is the major channel of the C_2H_2 + O(^{3}P) reaction.[3−5] The rate constants of R1a and R1b are found to be 2.23×10^{-14} and 8.95×10^{-14} cm^3 molecule^{-1} s^{-1}, respectively. The ketenyl radical reacts with O(^{3}P) by a fast process to produce CO ($k = 1.3 \times 10^{-10}$ cm^3 molecule^{-1} s^{-1})[5] and CO_2 (8×10^{-12} cm^3 molecule^{-1} s^{-1})[6] with large exothermicities.

$$HCCO + O(^3P) \rightarrow 2CO + H \quad (-102 \text{ kcal/mol}; -428 \text{ kJ/mol}) \quad \text{(R2a)}$$

$$\rightarrow CO_2 + CH(X^2\Pi) \quad (-54 \text{ kcal/mol}; -227 \text{ kJ/mol}) \quad \text{(R2b)}$$

Similar to the ketenyl radical, the triplet methylene radical may react with O(^{3}P) according to

$$CH_2(^3B_1) + O(^3P) \rightarrow CO + 2H \quad (-74 \text{ kcal/mol}; -311 \text{ kJ/mol}) \quad \text{(R3a)}$$

$$\rightarrow CO + H_2 \quad (-178 \text{ kcal/mol}; -748 \text{ kJ/mol}) \quad \text{(R3b)}$$

The rate constants for R3a[7] and R3b[7] are 7.8×10^{-11} and 5.2×10^{-11} cm^3 molecule^{-1} s^{-1}, respectively.

There are numerous studies establishing the branching ratio and rate constants of the C_2H_2 + O and the HCCO + O reactions.[3,5,8−10] However, only a few studies focus on the energy disposal of these reactions.[4,11,12] Schmoltner et al.[4] studied the C_2H_2 + O(^{3}P) reaction in a crossed molecular beam apparatus, measuring the translational energy distribution of the HCCO and the CH_2(^{3}B) products. Their results indicate that, for both channels, R1a and R1b, the largest fraction of the available energy is deposited into the translational degree of freedom. This suggests there is an exit channel barrier for both channels. The exact translational energy could not be determined in those experiments because of the insensitivity of the instrument at higher translational energies. A study by Shaub et al.[13] investigated the nascent vibrational distribution of the CO product of R1a at relatively high pressures (10 Torr) by using the CO laser resonant absorption technique. It was concluded that there is a small contribution to the observed CO signal from R3, but the R1b channel was considered to be a minor channel at the time of the experiment[14−16] and thus the HCCO + O(^{3}P) sequential reaction was not investigated. However, the most recent experimental determinations of R1a and R1b[3−5,17] indicate that R1b is the major channel. The branching ratio of R1b is close to 80% and is quite independent of the temperature. The room temperature rate constant mea-

* To whom correspondence should be addressed.

10.1021/jp040585+ CCC: $30.25
Published on Web 02/23/2005

surements indicate that the R2a channel is ~85%.[8,9] These data are supported by RRKM calculations[12] by Wagner and Harding. Thus, the most likely secondary reaction in the $C_2H_2 + O(^3P)$ system is HCCO + $O(^3P)$ to produce CO(v).

This paper describes measurements of the nascent vibrational distributions of CO(v) from both R1a and R2a using infrared emission from the CO products. The $O(^3P)$ and the HCCO reagent are generated by several different methods to minimize contributions from other possible reactions to establish the dynamics of these reactions. Both reactions have some contributions of CO(v) from competing processes, and thus, there are some limits on the accuracies of the determinations. It is found that the CO vibrational distribution of R1a agrees well with the previous experiment by Shaub et al.[13] In addition, the vibrational distribution of CO from R2a is determined for the first time. The nascent vibrational distribution of R1 has a contribution from a secondary reaction whose distribution agrees well with that of CO(v) observed more directly from the HCCO + $O(^3P)$ reaction (R2a). The results for HCCO + $O(^3P)$ have less than 10% contributions due to the $C_2H_5 + O(^3P)$, when ethyl ethynyl ether is used as the HCCO precursor. The CO(v) vibrational distributions from both title reactions fit nearly Boltzmann-like temperatures or two-component temperatures, which are in agreement with proposed longer-lived intermediate mechanisms, as opposed to direct mechanisms. The bimodal distribution of the HCCO + $O(^3P)$ reaction strongly suggests that the reaction proceeds through a $HC(O)CO^{\ddagger}$ complex, which decomposes into two CO molecules in a sequential process.

Experimental Section

Infrared emission from a chemical reaction is a very powerful tool to identify vibrationally excited products and to learn about their state distributions. The infrared emission can be detected by a Fourier transform spectrometer, which offers superior throughput and resolution over conventional grating spectrophotometers. The Fourier transform infrared (FTIR) instrument coupled with pulsed lasers allows the experimentalist to obtain time information and gain insight into the mechanisms of the reactions of interest. This is done by using a step scan FTIR apparatus, which permits high time resolution data to be obtained, limited only by the pulse width of the laser and the speed of the detection electronics. At moderately low pressures, this technique gives important information about elementary reaction steps and their vibrational, rotational energy transfer processes.

Time-Resolved Experiments. The experimental apparatus used in this study was described previously in detail.[18] Briefly, the reaction takes place in a vacuum chamber pumped by a 1000 L/s capacity Roots blower pump backed by an 80 L/s capacity mechanical pump. For the time-resolved experiments, the reagents are generated and reacted in two different reactors, shown in Figures 1a and b, which each has its own advantages.

Figure 1a depicts a segregated photolysis zone reactor (reactor 1), which allows the study of radical−molecule reactions. In this study, SO_2 is photolyzed by a 193 nm excimer laser and the resulting $O(^3P)$ radical flow intersects the C_2H_2 flow, where the reaction and observation take place in the interaction zone of the FTIR instrument. The overall reaction rate is governed in this reactor by the rate constants of the reactions and the mixing time of the initial reagents. The C_2H_2 inlets are tilted 45° to each other in order to efficiently intersect the $O(^3P)$ flow generated from the photolysis of SO_2. Argon is introduced into the chamber to keep the optics and the windows clean. Typical pressures in the experiment are 300 mTorr (40 Pa). The

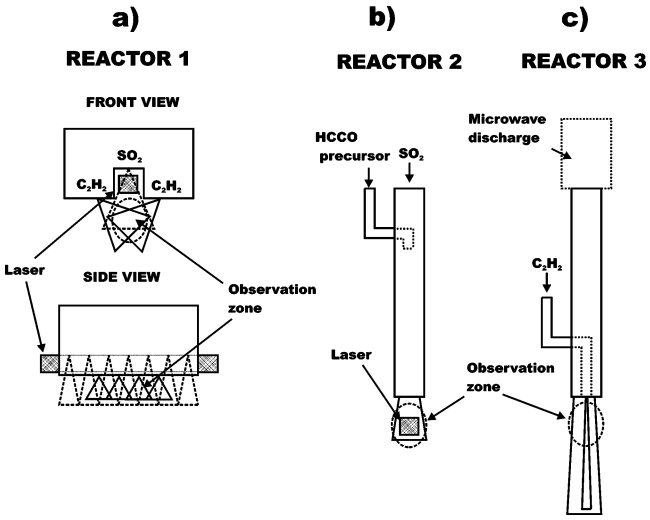

Figure 1. Simplified schematic of the three reactors used in this study: (a) Separate excitation reactor. This reactor allows the time-resolved study of radical−molecule reactions by the separate generation of a radical precursor with a laser pulse. (b) Radical−radical reactor. The flows of radical precursors are mixed upstream in a stainless steel tube and photolyzed simultaneously in the observation zone of the FTIR instrument. (c) Microwave discharge reactor. The $O(^3P)$ atoms are generated in a microwave discharge from high flow velocity O_2 and combined with the C_2H_2 flow in the observation zone of the FTIR instrument.

pressures have to be kept relatively low (below 500 mTorr; 67 Pa) in order to minimize the introduction of the other reagent, in this case acetylene, in the photolysis region, thereby producing unwanted radicals, such as C_2H. To find the optimal conditions under which the precursors can be kept spatially separated, the effectiveness of the spatial separation is checked by introducing ammonia (into the acetylene inlet in Figure 1a), which produces electronically excited NH_2 very efficiently and is a strong emitter. The SO_2 inlet is balanced with argon with the same flow rates used in the ammonia experiments to imitate the same fluid dynamics in the chamber. No signal could be observed from NH_2*, which is a good indication that no photolysis of C_2H_2 can occur under the conditions described in this study, thus ensuring the absence of C_2H from 193 nm photolysis under these conditions. In addition, reactor 1 has the advantage that the radicals prepared by photolysis with the laser have time to relax into their ground state before they intersect the C_2H_2 flow and the viewing region. Under the experimental conditions, a time of ~10−15 μs for intersection is determined by introducing NH_3 through the SO_2 inlet indicated in Figure 1a.

Figure 1b shows another reactor (reactor 2) in which radical−radical reactions can be studied by photolyzing a homogeneous mixture of radical precursors. Ethyl ethynyl ether ($HCCOCH_2CH_3$) and SO_2 are mixed upstream to ensure the homogeneous mixing of the precursor molecules. The photolysis of ethyl ethynyl ether and the SO_2 efficiently produces HCCO radicals and $O(^3P)$, respectively. The absorption cross section of the ethyl ethynyl ether is $\sim 7 \times 10^{-18}$ cm^2/molecule at 193 nm. The 193 nm photolysis of ethyl ethynyl ether produces HCCO + C_2H_5 radicals with a quantum yield near unity.[19] The ethyl ethynyl ether is dissolved in hexane solution and is seeded into a small flow of He into the reactor. The hexane stabilizer has a negligible absorption cross section at 193 nm ($\sim 3 \times 10^{-22}$ cm^2/molecule). The absorption cross section of SO_2 is $\sim 6 \times 10^{-18}$ cm^2/molecule at 193 nm and produces $O(^3P)$ efficiently. The total pressure in the chamber is 1.5 Torr.

Microwave Discharge Experiment. Figure 1c shows a reactor used in the microwave discharge experiments (reactor

3). The microwave discharge of oxygen molecules takes place in a quartz tube, efficiently producing $O(^3P)$ atoms. The $O(^3P)$ atoms are mixed downstream with a flow of C_2H_2. The acetylene flow is kept relatively low compared to the O_2 flow, so the flow does not become divergent. The microwave discharge apparatus has a limited time resolution, which is determined by the residence time of the reaction products in the observation zone of the collection optics. The residence time of the products can be significantly reduced by using high flows of the reagents and balancing the pressures outside the flow region with a buffer gas, ensuring the spatial collimation of the flow and further reducing the residence time. The residence time is checked by introducing a small amount of acetone into the flows and photolyzing them with a 193 nm laser. The relatively long lifetime of the vibrationally excited CO (~33 ms) allows an estimate of the residence time of the molecules in the observation zone. Typical residence times in these experimental conditions can range from 50 μs to ~2 ms. These values correlate well with the residence times determined from the mass flow velocities. To keep the pressures low to reduce the possibility of collisional relaxation of the vibrationally excited products, the pumping capacity is set to the maximum of the Roots blower.

The IR radiation produced by the chemical reactions is collected by Welsh cell optics, exits the vacuum chamber through a CaF_2 window, and enters the FTIR instrument. The infrared radiation is collimated and focused on the entrance port of the FTIR spectrophotometer, matching its *f* number (4.5). An iris is placed in front of the spectrometer to reduce the field of view and to achieve the desired spectral resolution. The commercially available vacuum FTIR spectrometer can analyze both time-resolved and static signals. The signals are detected by liquid nitrogen cooled indium antimonide (InSb) or mercury cadmium telluride (MCT) detectors. The InSb detector ($D^* \cong 2.2 \times 10^{11}$ cm $Hz^{1/2}$ W^{-1}) has a higher sensitivity than the MCT detector ($D^* \cong 3.8 \times 10^{10}$ cm $Hz^{1/2}$ W^{-1}), but its response curve falls off at around 1800 cm^{-1}. The MCT detector has a better spectral range (lower limit ~1000 cm^{-1}), but it is not sensitive enough to get high resolution spectra within reasonable data acquisition times for this experiment. Thus, it is used for low resolution spectra when longer wavelengths are desired. The detected signal is amplified and digitized to obtain the interferograms.

The commercially available acetylene (99.6%) used in these experiments is purified with an activated carbon trap in order to remove the residual acetone from the reagent flow. The trap is evacuated overnight before each experiment to ensure efficient removal of the acetone. The $O(^3P)$ is produced by the photolysis of SO_2 (anhydrous, 99.98%). The ethyl ethynyl ether is commercially available as a 40% solution in hexane. Pressure is measured using capacitance manometers. The gas flows are regulated by needle valves and measured by standard calibrated mass flow meters.

Results and Discussion

Time-Resolved Study of the C_2H_2 + $O(^3P)$ Reaction. Time-resolved spectra of the CO and CO_2 products are observed by reactor 1. It was pointed out above that this reactor can selectively produce $O(^3P)$ radicals and eliminate the possibility of C_2H radical formation in the photolysis step, which would ordinarily lead to fast reaction with $O(^3P)$, producing interfering CO and CO_2 in the reaction system. In addition, reactor 1 facilitates the relaxation of electronically and vibrationally excited reagent molecules, since the mixing and reaction take place ~10 μs after the photolysis of the precursor molecules. Because of the complex flow dynamics and delayed mixing, the time history of the signals is not readily correlated with straightforward expectations for the kinetics, as will be seen below.

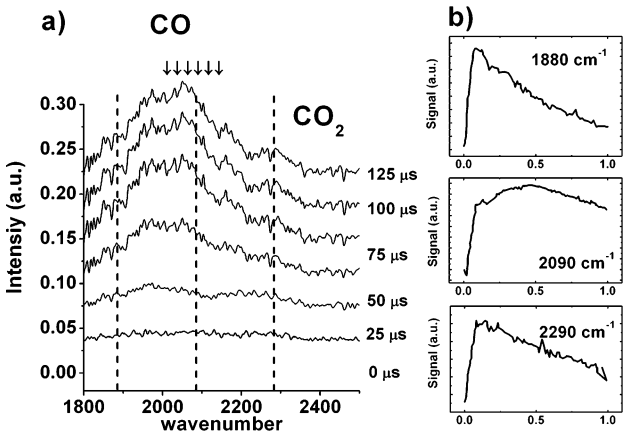

Figure 2. (a) Time-resolved IR emission spectra of the C_2H_2 + $O(^3P)$ reaction process with initial reagent pressures of $p(SO_2)$ = 18 mTorr (2.4 Pa) and $p(C_2H_2)$ = 12 mTorr (1.6 Pa). The total pressure is 300 mTorr (40 Pa) with the balance due to Ar in the detection volume of the instrument. The laser fluence is 150 mJ cm^{-2} $pulse^{-1}$. The data are taken by an InSb detector at 8 cm^{-1} spectral resolution and 5 μs temporal resolution. The observed products are CO and CO_2 and are indicated on the figure. The positions of the $J = 0 \rightarrow 0$ vibrational transitions are indicated on the graph with a series of vertical arrows up to $v = 6$ ($v = 6$ is to the left), which corresponds to the maximum available energy for CO(v) from C_2H_2 + $O(^3P)$. (b) The time evolution of the CO signal from Figure 2a at 1880, 2090, and 2290 cm^{-1}

Several low resolution time-resolved emission spectra taken at 25 μs intervals are shown in Figure 2. The major product is vibrationally excited CO, which has a broad emission feature in the low resolution spectra between 1800 and 2250 cm^{-1}. It is possible that the CO emits a small amount below 1800 cm^{-1}; however, the InSb detector spectral cutoff frequency is at ~1800 cm^{-1}, so emission at lower energies is not obtained. A smaller amount of vibrationally excited CO_2 product is also observed at ~2300 cm^{-1}, which persists on a similar time scale as the CO product.

The kinetics of the CO and CO_2 products is investigated at 1880, 2090, and 2290 cm^{-1}. All of these data show somewhat similar rise times, but they are not simple exponentials and there are secondary minima and maxima; these are most likely a result of multiple factors: the reaction rate, flow mixing of the reagents, and vibrational deactivation initially with radicals and later with molecules. The reagent mixtures from this reactor are not homogeneous, and the relative reagent concentrations vary significantly in the observation zone with time. The kinetics at these frequencies show very different behaviors. The 1880 and 2290 cm^{-1} data are nearly superimposable. The 2090 cm^{-1} data seem to show one part that is nearly the same kinetics as that at 1880 and 2290 cm^{-1}, but in addition, there is a slower process producing CO at that wavelength. The 1880 and 2290 cm^{-1} kinetics data suggest that there is one process that produces the simultaneous CO and CO_2 vibrationally excited products. The HCCO + $O(^3P)$ reaction has been shown to produce a significant amount of CO_2 beside CO.[6] Also, in Figure 2a, the vibrational transitions of the CO are indicated by arrows from $v = 1$ to $v = 6$ for CO(v) from the C_2H_2 + $O(^3P)$ reaction (right to left). Because of the extended vibrational excitation and the CO_2, the spectra indicate that some other reaction has to contribute to the observed signal. On the basis of kinetic

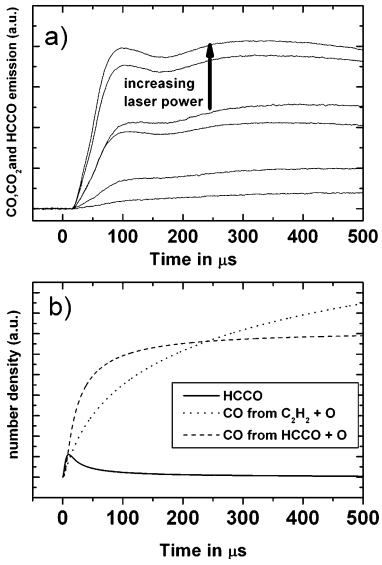

Figure 3. (a) Power dependence of the CO and CO_2 (and HCCO) emission taken with an interference filter. The initial reagent pressures are the same as those in Figure 2. The laser fluences are 34, 58, 90, 117, 135, and 153 mJ cm^{-2} $pulse^{-1}$, respectively. (b) Simulation of the kinetics of CO and HCCO products using the known rate constants for R1−R3 including the known SO + O recombination rate ($k = 5.3 \times 10^{-11}$ cm^3 $molecule^{-1}$ s^{-1}) and assuming a reaction rate constant ($k = 3 \times 10^{-10}$ cm^3 $molecule^{-1}$ s^{-1}) for HCCO + SO_2 and/or HCCO + C_2H_2 reactions.

considerations, the HCCO + $O(^3P)$ is the most likely contributor. The 2090 cm^{-1} data show CO production with a lower exothermicity than that of the HCCO + $O(^3P)$ reaction. The most obvious candidate to explain this reaction channel is the C_2H_2 + $O(^3P)$ reaction. This reaction is a fairly slow process compared to the HCCO + $O(^3P)$ reaction. Since HCCO can only be produced first by C_2H_2 + $O(^3P)$, the sequential kinetics of HCCO should be a double exponential with inverted order. Thus, the HCCO + $O(^3P)$ time constant can appear first in the signals. The secondary minimum may be due to an initial rapid relaxation of CO(v) by O, followed by slower vibrational deactivation of CO(v) when the O atom concentration decreases.

Figure 3 shows the laser power dependence of the combined CO and CO_2 time-resolved emission signals transmitted by an interference filter (spectral range 1800−2500 cm^{-1}) and the same reactor used above (reactor 1). Similarly to the data shown in Figure 2b, the kinetics of the sum of the CO and CO_2 signals shows a double maximum type kinetic curve. Even though this signal does not adhere to conventional kinetic expectations, the first rise is suggested to be primarily from the kinetic effect of the HCCO + $O(^3P)$ reaction, resulting in CO and CO_2 products, and the second from the C_2H_2 + $O(^3P)$ reaction, resulting in CO. Naturally, the first rise must also have a substantial C_2H_2 + $O(^3P)$ contribution to the CO signal. The laser power dependence has a quadratic effect on the initial rise time, suggesting that the HCCO + $O(^3P)$ reaction plays a large role in that part of the signal. However, quantitatively, this is subtle because the vibrational deactivation of CO(v) by O and other radical species has a complicated effect on the kinetics, since the radical concentration rapidly changes.

The reagent concentrations are chosen in this experiment so the kinetics data from the emission through the interference filter produce the double peak behavior in order to demonstrate the two different processes (R1a and R2a) that result in CO(v) in the C_2H_2 + $O(^3P)$ system. The kinetics behavior is assigned on the basis of the observed vibrational distribution of CO(v) and its power dependence. Qualitative understanding of the kinetics of the observed signal can be obtained by simulating the reaction system (R1−R3) using the known rate constants and the concentrations used in Figure 2. The simulated time evolutions of CO, CO_2, and HCCO radicals are shown in Figure 3b. To simulate better the signal appearance in the observation zone and include the mixing of the initial reagents, the acetylene initial concentration is taken as a variable, which is assigned to its maximum after 10 μs. This is done to account for the physical picture that the photolysized SO_2 flow gradually moves and mixes into the acetylene flow in the observation zone. The initial concentration of $O(^3P)$ is determined by the absorption cross section of SO_2 (6×10^{-18} cm^2/molecule).[20,21] The filter kinetics data show a dip in Figure 3a, which does not show up in Figure 3b. This is either due to the mixing nonidealities mentioned above or to vibrationally excited HCCO,[22] which forms in the first step of the reaction. The HCCO species was also reported[23,24] centered around 2023 cm^{-1}. The deactivation of the HCCO would mainly be due to the HCCO + $O(^3P)$, HCCO + SO_2, and HCCO + C_2H_2 reactions. Quantitative comparison is difficult due to the concentration inhomogenities in the observation zone, the lack of knowledge of quenching rate constants of the HCCO, and the difficulty directly relating the observed signal to concentrations (it requires the knowledge of the population distributions and Einstein A coefficients for all species present).

The following conclusions can be drawn from the above results. The vibrationally excited CO(v) shows higher exothermicity than what is expected from only the C_2H_2 + $O(^3P)$ reaction, which strongly suggests the sequential process is an important contributor to the observed CO distribution. Previous results and the observation of the CO_2 strongly suggests that the HCCO + $O(^3P)$ reaction is the major sequential reaction under the experimental conditions. No quantitative high resolution data could be obtained due to the low signal levels. To overcome the experimental difficulties, a different reactor and detection mode is used, which is discussed below.

C_2H_2 + $O(^3P)$ Reaction in the Microwave Discharge Reactor. The difficulty with the $O(^3P)$ production by 193 nm photodissociation of SO_2 is that it may lead to other radicals and reagents that can contribute to the reaction of interest. To minimize possible contributions from SO and SO_2, and to identify other possible products such as CH, an alternative, cleaner source of $O(^3P)$ is obtained by microwave discharge of O_2 at low pressures.[25] These experiments do not permit the pulsed time-resolved capability of the FTIR instrument. This source may also produce O_3 and contain O_2, which could react with HCCO, but at lower rates than the HCCO + $O(^3P)$ reaction.[5,26−28] Although the time information of the microwave apparatus is somewhat reduced, for a reaction such as C_2H_2 + $O(^3P)$ at fast flow rates of reagents and low pressures, the residence time of the vibrationally excited photoproducts is short enough to obtain a nascent or close to nascent vibrational distribution of the CO(v) photoproduct. The estimated $O(^3P)$ fraction in a typical O_2 flow at the pressures used in this study is <1%.[25] Since the reaction takes place in a large excess of acetylene ($[C_2H_2] \gg [O]$), this somewhat minimizes the secondary reactions, but not completely.

The determination of the nascent vibrational distribution of CO(v) from any reaction requires that the vibrational deactivation rate is negligible. The rate constants for the following processes can be used for CO($v = 1$) + M → CO($v = 0$) + M, where M corresponds to the molecules present in the reaction system. A typical reaction mixture consists of 40 mTorr (5.3 Pa) of Ar or N_2, 172 mTorr (22.9 Pa) of O_2, and 12 mTorr (1.6

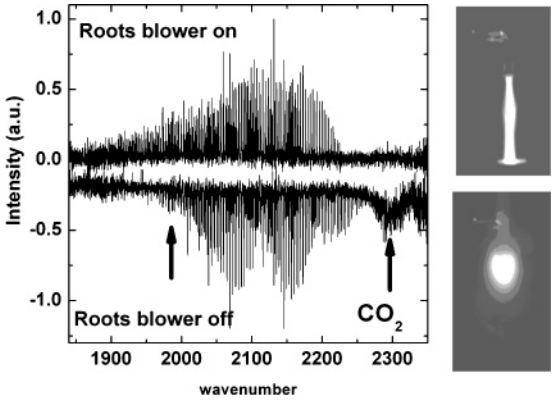

Figure 4. Effect of the flow rate (residence time) on the product distribution of CO from C_2H_2 + O(^{3}P) and HCCO + O(^{3}P). The "Roots blower on" indicates the high flow rate (short residence time in the observation zone). The "Roots blower off" corresponds to low flow rate (long residence time in the observation zone). On the right side, a photo of the visible emission of the triplet CO[42,43] in the interaction zone is shown.

Pa) of C_2H_2. The best values of vibrational relaxation rate constants for CO(v = 1) with these molecules are the following: 2.4×10^{-16} cm^3 molecule^{-1} s^{-1} (Ar),[29] 5.46×10^{-15} cm^3 molecule^{-1} s^{-1} (N_2),[30] 1.5×10^{-15} cm^3 molecule^{-1} s^{-1} (O_2),[31] and 2.1×10^{-13} cm^3 molecule^{-1} s^{-1} (C_2H_2).[32] Simple consideration of the concentration and deactivation rates leads to the conclusion that the most important molecule in the deactivation of CO(v) is the C_2H_2 in this system. Variation of the C_2H_2 concentration in the present setup is difficult without influencing the residence time or losing spectral resolution due to less signal. Fortunately, Wang et al.[32] investigated the CO(v = 1) + C_2H_2 → CO(v = 0) + C_2H_2 relaxation process in a time-resolved FTIR setup very similar to the one used in this experiment, observing the above process in a few hundred microsecond time scale. In their experiment, the pressure of the C_2H_2 is ~40 times higher than that in the present experiment (487 mTorr compared to 12 mTorr). This difference would lead to 40 times slower vibrational relaxation of CO(v) by C_2H_2. For our residence times as short as 50 μs, this strongly suggests that the observed CO(v) corresponds to a near-nascent CO distribution for the reaction(s).

The effect of the flow rate of the reagents is demonstrated in Figure 4. The upper part of the graph shows the vibrationally excited CO product spectrum obtained with a high flow rate and a short observation time. The inverted curve shows the data obtained with significantly reduced flow rates. Both spectra are taken at the same total pressure (700 mTorr; 93.3 Pa). To keep the pressure the same, the Roots blower had to be switched off. The total flow rates of O_2 plus C_2H_2 are 1653 and 204 sccm when the Roots blower is on and off, respectively. This results in a reduction of residence time by a factor of 8; however, the actual residence time when the Roots blower is off is much larger due to the lost collimation of the flow (see Figure 4, lower right). The difference in pumping capacity of the Roots blower versus the backing pump is 1000 L/s versus 60 L/s, which would indicate a factor of 15 reduction of the residence time.

There are two main differences between the lower and upper spectra of Figure 4. The first one is the formation of CO_2, which is expected from the HCCO + O(^{3}P) reaction (or from HCCO + O_2). The second difference is that the CO on the inverted spectrum reflects vibrationally relaxed CO, indicated by the large amount of population at the v = 1 level (the center of v = 1 is located at 2143 cm^{-1}) and the reduced intensity of the higher CO transitions at 1900 cm^{-1}. Even though the HCCO + O(^{3}P) and CH_2 + O(^{3}P) reactions are minimized in the high flow rate

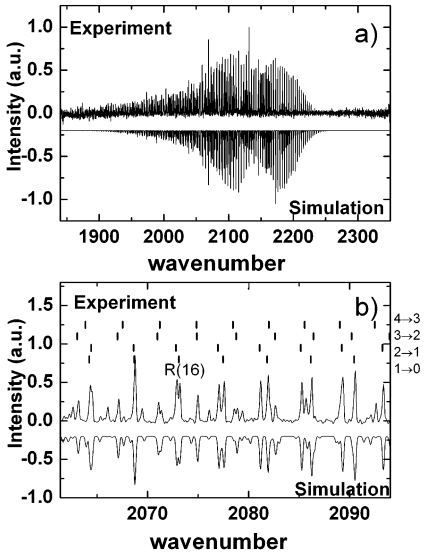

Figure 5. (a) Experimental and simulated spectra of the CO(v) vibrational distribution from C_2H_2 + O(^{3}P) with a small secondary contribution due to the HCCO + O(^{3}P) reaction. The data are taken with the microwave discharge apparatus at a 0.15 cm^{-1} spectral resolution. The flow rates of O_2, C_2H_2, and Ar are 1400,100, and 200 sccm, respectively, and p(total) = 225 mTorr (30 Pa). The simulated spectrum is inverted for better visibility. (b) Expanded section of the graph of Figure 5a. The positions of the four vibrational transitions are indicated on the graph with a series of vertical arrows.

(short observation time) data, it will be shown below that there is some contribution from these reactions to the observed CO(v) emission.

Analysis of the Product Distribution of the C_2H_2 + O(^{3}P) Reaction. To extract the vibrational distribution of the vibrationally excited CO products, a spectral simulation and fitting is done. The good S/N data in the microwave discharge experiment allow high spectral resolution data (nominal resolution 0.115 cm^{-1}) to be obtained, which helps to identify the spectral positions very accurately. The simulation program creates the line positions by using the published spectroscopic constants of CO.[33] The line intensities are generated by assuming a population at each rovibrational level, and then it is multiplied by the Einstein A coefficient[34] for the rovibrational transitions according to the following equation:

$$N(J', v') = \frac{I''^{J'\rightarrow J''}_{v'\rightarrow v''}}{A''^{J'\rightarrow J''}_{v'\rightarrow v''}(2J'+1)}$$

The resulting stick spectrum is convolved with the instrument response function, which describes the broadening and the shift associated with the field-of-view error.[35] The field-of-view error can be calculated from the resolving power of the instrument at a given aperture setting according to $R \cong 8F^2/h^2$, where F (100 mm) is the focal length of the instrument and h (2.5 mm) is the diameter of the aperture. The calculated spectral resolution is 0.156 cm^{-1}, which is in good agreement with the measured line width (0.15 cm^{-1}) at 2000 cm^{-1}. During the fitting process, the populations of the rotational levels are assumed to be Boltzmann-like, so each vibrational level has two input parameters: the vibrational population and the rotational temperature. The rotational temperatures of the vibrational populations have been found to be ~500 ± 50 K. This higher rotational temperature suggests that the rotational populations are not completely equilibrated; however, using a Boltzmann-like distribution results in an excellent fit. Figure 5 shows the

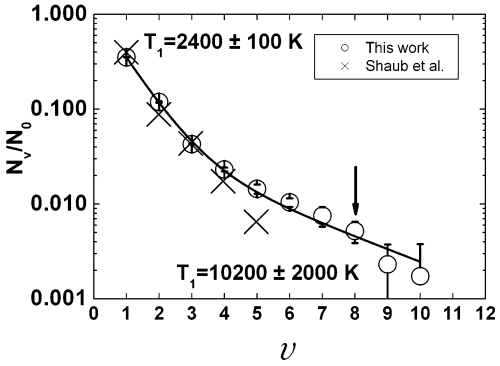

Figure 6. Experimentally determined nascent distribution of CO(v) from the $C_2H_2 + O(^3P)$ reaction (open circles) using the microwave discharge apparatus. The solid line indicates the fitting of the experimental nascent distribution with a linear combination of two exponentials. The vibrational temperatures are found to be 2400 ± 100 and 10 200 ± 2000 K. The maximum available energy for CO from the $C_2H_2 + O(^3P)$ reaction is indicated by an arrow. The previously determined nascent vibrational distribution for R1a is also shown (crosses).

experimental CO spectrum and the fitted simulated spectrum. The upper curve shows the whole spectrum, and the lower graph is a magnification of the data and simulation. The relative error bars are estimated by observing the deviation in the error function upon changing the fitting parameters.

The measured vibrational distribution of CO(v) from the $C_2H_2 + O(^3P)$ reaction is shown in Figure 6. The ground state population ($v = 0$) of CO from this reaction is not known. To accurately normalize the data, the first three points of the vibrational distribution are used by linear extrapolation to predict the ground state population. A surprisal analysis is not used because of complications with the interfering secondary reactions described below. The resulting nascent vibrational distribution for $v = 1-5$ agrees well with the earlier results by Shaub et al.[13] In that work, the CO populations were extracted from time-resolved infrared absorption data, extrapolating the data to zero time. In that way, the CO from secondary reactions is eliminated from their results. The discharge flow method however does not have sufficient time resolution, so secondary reactions do contribute to the CO distribution. To obtain a vibrationally unrelaxed CO(v) distribution, although contaminated by secondary reactions, several steps are taken. First, the pressures in the reaction chamber are kept low to reduce the number of collisions. This is achieved by using the full capacity of the Roots blower pump. Second, the reagent flows are kept high in order to reduce the residence time in the observation zone. In addition, the collimation of the reagent flow is important. If it is not collimated, this might reduce the effective flow rate. Collimation can be achieved by balancing the pressures outside the interaction zone with a buffer gas. The average residence time is measured by photolyzing acetone, which very effectively produces vibrationally excited CO, and this emission provides a convenient way to measure the residence time in the observation zone. The typical residence times are found to be between 50 and 2000 μs depending on the conditions. In most experiments, a residence time shorter than 100 μs is used. It is important to point out that the reactor used in the microwave discharge experiment (Figure 1b) has the advantage that the reactants are not well mixed, resulting in a relatively slow reaction, which increases the possibility that the observed vibrationally excited CO during the observation time is less contaminated by secondary reactions.

Despite these precautions, the observed vibrational distribution of CO(v) from the $C_2H_2 + O(^3P)$ system shows a bimodal distribution in Figure 6. On the basis of the comparison with previous results[13] and the reaction exothermicities (the maximum v for $C_2H_2 + O(^3P)$ is $v = 8$), it is clear that the observed nascent distribution in our microwave discharge apparatus has to have a contribution from some other reaction. The lowest vibrational states have identical distributions to those of Shaub et al.,[13] obtained with a separate experimental technique and under different conditions. Their work concluded that the major observed channel is R1a and there is some contribution from the $CH_2(^3B) + O(^3P)$ reaction; however, at the time of their experiment, reaction R1b was considered to be insignificant compared to R1a. On the basis of the rate constants known now, it is more likely that the additional contribution to the vibrationally excited CO comes mostly from the HCCO + $O(^3P)$ reaction and not from the $CH_2(^3B) + O(^3P)$ reaction. Since the rate constants of R2a ($k = \sim 1.3 \times 10^{-10}$ cm^3 molecule^{-1} s^{-1})[5] and R3 ($k = \sim 1.3 \times 10^{-10}$ cm^3 molecule^{-1} s^{-1})[36] are very close to each other, the amount of vibrationally excited CO is entirely determined by the branching ratio between R1a and R1b and the fact that HCCO + $O(^3P)$ produces two CO molecules and $CH_2 + O(^3P)$ produces only one. If the vibrational distributions of these two reactions were similar, the contribution to the CO signal from $CH_2(^3B) + O(^3P)$ would be around 12% of the HCCO + O reaction at maximum.

If we assume that the "hot" part of the vibrational distribution entirely comes from the HCCO + $O(^3P)$ reaction and the vibrationally "cold" part is a result of the $C_2H_2 + O(^3P)$ reaction, the nascent distribution of both the $C_2H_2 + O(^3P)$ and HCCO + $O(^3P)$ reactions could in principle be determined in a single step. However, the built-in assumption is that the HCCO + $O(^3P)$ reaction does not contain any cold part but can be characterized by a single Boltzmann-like distribution. It will be shown in the next section that this is not the case; that is, CO(v) from HCCO + $O(^3P)$ does have a bimodal distribution, and therefore, some CO(v) from HCCO + $O(^3P)$ interferes with the cold part of the $C_2H_2 + O(^3P)$ distribution observed here.

Time-Resolved Study of the HCCO + O(^{3}P) Reaction. To relate further the vibrational distribution of CO in Figure 6 partially to the HCCO + $O(^3P)$ reaction, a time-resolved FTIR experiment is carried out using reactor 2 in Figure 1b. For the HCCO precursor, ethyl ethynyl ether ($HCCOCH_2CH_3$) is used, which produces HCCO and ethyl radicals with nearly 100% quantum yield at 193 nm photolysis. The vibrational distribution of CO from the ethyl + $O(^3P)$ reaction has been previously determined[37] and shows a much cooler vibrational temperature than that expected from the HCCO + $O(^3P)$ reaction. For the $O(^3P)$ precursor, SO_2 is used, which produces $O(^3P)$ very effectively. The laser fluences are lowered until no CO from the ethyl ethynyl ether photodissociation is observed alone (~35 mJ cm^{-2} pulse^{-1}), to minimize the subsequent photodissociation of HCCO[38,39] to CO and CH.

Figure 7 shows a small section of the CO(v) spectrum obtained from the HCCO + $O(^3P)$ and ethyl + $O(^3P)$ reactions at a 15 μs time delay along with the simulated spectrum. The simulation is carried out in an identical manner to that previously described in the microwave discharge experiment. The obtained vibrational distribution of CO shows a bimodal behavior in Figure 7b. The data points in the figure are fitted with a linear combination of two exponentials (straight lines in the log plot) to extract vibrational temperatures. The underlying assumption in this procedure is that there are two physical processes and each of these processes yields a Boltzmann-like vibrational distribution for CO(v). The vibrational temperatures are found to be 2320 ± 40 and 10 300 ± 600 K. The 10 300 K value is

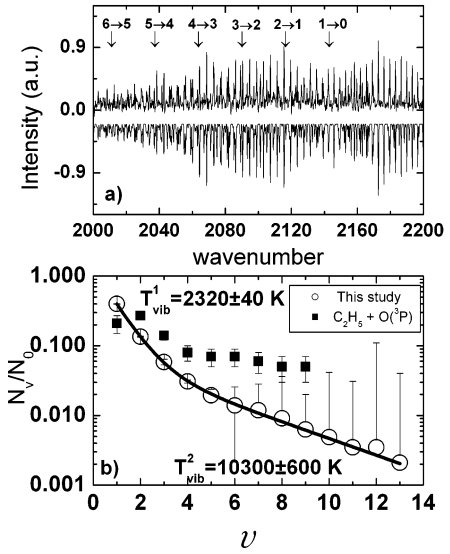

Figure 7. (a) Experimental and simulated spectrum of the CO vibrational distribution from HCCO + $O(^3P)$ using the reactor in Figure 1b and the time-resolved apparatus. The data are taken with the high sensitivity, but limited spectral range InSb detector (see text) at a 0.2 cm^{-1} spectral resolution at a 15 μs time delay after the laser pulse. The ethyl ethynyl ether seeded into a 100 sccm flow of He combined with 125 sccm of SO_2 and combined with 2000 sccm of Ar flow (p(total) = 1500 mTorr; 200 Pa). The laser fluence is 35 mJ/cm^2. The simulated spectrum is inverted for better visibility. (b) Experimentally determined nascent distribution of CO(v) from the HCCO + $O(^3P)$ reaction (open circles) from the time-resolved 193 nm photodissociation of ethyl ethynyl ether and SO_2. The solid line indicates the fitting of the experimental nascent distribution with a linear combination of two exponentials. The vibrational temperatures are found to be 2320 ± 40 and 10 300 ± 600 K.

in good agreement with one of the vibrational temperatures observed in the microwave discharge experiment (10 200 K). The vibrationally colder part (2320 K) of the vibrational distribution comprises a relatively small number of vibrational levels; it does not agree well with the expected amount and distribution of CO from the ethyl + $O(^3P)$ reaction.[37] The data are taken with an InSb detector, which has limited spectral range, and the highest observed vibrationally excited CO transition is found to be 13 → 12, which is somewhat less than the maximum available expected (up to 19 → 18) on the basis of the exothermicity for the HCCO + $O(^3P)$ reaction. To explore this, the same data are taken with the MCT detector with a lower spectral resolution shown in Figure 8. In this figure, the vibrational transitions of the CO ($J = 0 \rightarrow 0$) are indicated with vertical arrows from the 1 → 0 vibrational transition up to 19 → 18. The data are fitted with the simulated spectrum indicated by a dashed curve. The vibrational distribution obtained (not shown) is very similar to the distribution presented in Figure 7b but has larger error bars. In addition, the fit clearly indicates that the vibrational distribution of CO(v) from the HCCO + $O(^3P)$ reaction extends up to the available exothermicity of this reaction.

An important question is how much the C_2H_5 + $O(^3P)$ reaction contributes to the measured CO(v) for the HCCO + $O(^3P)$ reaction. The total rate constant for the former reaction is 2.2×10^{-10} cm^3 $molecule^{-1}$ s^{-1}, reported by Slagle et al.[40] They indicate that 95% of this reaction results in three main channels, which do not contain any CO(v) as a primary product. Reid at al.[37] estimate that ~10% of the total rate for C_2H_5 + $O(^3P)$ results in CO(v). In that work, they use much higher concentrations of radicals than the present work and the products are detected by essentially the same experimental setup. Their

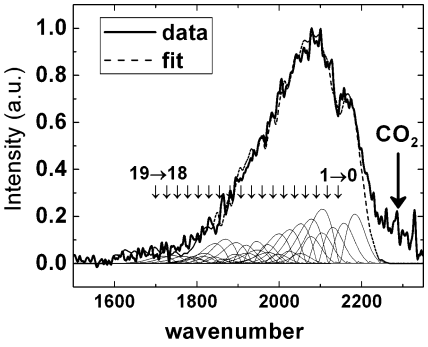

Figure 8. Experimental (solid line) and simulated (dashed line) spectra of the CO vibrational distribution from HCCO + $O(^3P)$ using the reactor in Figure 1b and the time-resolved apparatus. The data are taken with the lower sensitivity, but higher spectral range MCT detector (see text) at a 4 cm^{-1} spectral resolution and at 15 μs. The concentrations are the same as those in Figure 8. The positions of the $J = 0 \rightarrow 0$ vibrational transitions are indicated on the graph with a series of vertical arrows.

vibrational distribution for CO(v) from C_2H_5 + $O(^3P)$ is also shown in Figure 7b, which indicates that CO(v = 2) is much higher than CO(v = 1); this is very different from what is observed at present. They observe other products for the major channels of the C_2H_5 + $O(^3P)$ reactions such as H_2CO and OH (including the reagent CH_3CH_2 radical) with comparable intensity to the vibrationally excited CO product. In the present work, none of these products or precursor molecules are detected except vibrationally excited CO, which leads to the conclusion, under the experimental conditions in this work, that the observed vibrational distribution can be attributed to HCCO + $O(^3P)$ with a maximum error of ~10%. Recently, the total rate constant for C_2H_5 + $O(^3P)$ was measured[41] to be 1.7×10^{-10} cm^3 $molecule^{-1}$ s^{-1} by a discharge flow reactor at room temperature, which further lowers the relative contribution of the C_2H_5 + $O(^3P)$ reaction to the observed CO(v). The maximum available energy of R2a (HCCO + O → 2CO + H) is 36 580 cm^{-1}, which limits the maximum observable vibrationally excited CO to the 19 → 18 transition (see Figure 8). In Figure 8, the arrows indicate the calculated vibrational transitions of the CO including the anharmonicity of the vibrations. The high v's cannot be produced by the C_2H_5 + $O(^3P)$ reaction, suggesting that HCCO + O is the major contribution to the observed CO(v) distribution. In principle, vibrational relaxation may contribute to the above-mentioned bimodal distribution, but it has been shown in the previous sections that the vibrational relaxation rates occur more slowly than the CO production rate. The data in Figure 7 are taken at 15 μs after the photolysis, but spectra taken at 5 and 10 μs are identical to the 15 μs spectrum, suggesting that the vibrational deactivation is not significant. To obtain a sufficient signal-to-noise ratio but to minimize the contribution of the CO(v) from the photodissociation of the HCCO by lowering the photolysis laser energy, only the 15 μs data are used to determine the vibrational distribution of CO(v) in Figure 7b. Also, the experiments at different time delays prove that the secondary reaction contributions to the observed distribution are not significant.

We consider whether the vibrational distributions obtained in the time-resolved and microwave discharge experiments can be fit with a linear combination of Boltzmann statistics using a single or bimodal temperature to describe each process. The first process is R1a that produces vibrationally excited CO in the C_2H_2 + $O(^3P)$ reaction. Previous work[13] has established that this reaction results in a simple Boltzmann distribution for this reaction. By fitting the microwave discharge results, it is found that at least two exponentials (two vibrational temperatures) are

required to adequately simulate the total CO(v) produced, because of the additional HCCO + O contribution. The lower vibrational temperature (2400 K) obtained in the fitting process agrees well with the previous work (3070 K); however, because the vibrational distribution of CO(v) from HCCO + O(^{3}P) shows a bimodal distribution, our observed distribution is not directly related to CO(v) from the C_2H_2 + O(^{3}P) reaction, but a linear combination of the two reactions. Since the Boltzmann temperature of the cold part of the microwave discharge experiment (2400 K) fortuitously matches very well with the Boltzmann temperature of the cold part of CO(v) from the HCCO + O(^{3}P) reaction (2320 K), and the difference should give the pure CO(v) distribution uniquely due to the C_2H_2 + O(^{3}P) reaction, the conclusion is that the real vibrational distribution is very similar to the cold part of the microwave discharge experiment. This latter result is supported by the previously determined vibrational distribution by Shaub et al. (3070 K). The higher vibrational temperature in Figure 6 corresponds to the vibrationally excited CO(v) primarily from R2a. This can be inferred by comparing the vibrationally excited CO distribution from the microwave discharge experiment (10 200 K; Figure 6) and the time-resolved photodissociation experiment of ethyl ethynyl ether (10 300 K; Figure 7).

The Mechanism of the C_2H_2 + O(^{3}P) Reaction. The available energy of the C_2H_2 + O(^{3}P) reaction resulting in the CO-producing channel (CH_2(^{3}B) + CO) is 47 kcal/mol. The energy channeled into CO(v) vibrations is calculated from $\langle E_v \rangle = \Sigma f_v E_v$, where $f_v = N_v/\Sigma_v N_v$ is the fractional population and E_v is the vibrational energy. On the basis of the results of the microwave discharge experiment and assuming $v \leq 5$, the fraction of energy deposited into vibrations is found to be only 3.5 kcal/mol. In this calculation, the anharmonicity of the CO vibrations is taken into account and the population of the ground vibrational energy level of CO is extrapolated from the Boltzmann plot using the vibrational temperature of R1a in Figure 6. This fraction of energy into vibration is only f_v = 0.074, which is less than the value $f_v^{stat} = 0.142$ calculated from equipartition theory. As a crude approximation, the products are expected to arise with the fraction of energy predicted by statistical theory minus the barrier height of the exit channel, which can explain the difference between the observed and predicted fractions of energy into CO vibration. Figure 9a shows the energy diagram of the C_2H_2 + O(^{3}P) reaction, taken from previous theoretical calculations.[4,11,12] The C_2H_2 + O(^{3}P) reaction is thought to proceed through two intermediate complexes, the diradical intermediate HCCHO(^{3}A″), which subsequently isomerizes to the H_2CCO(^{3}A″) radical intermediate or dissociates into HCCO + H. The isomerized H_2CCO(^{3}A″) can further dissociate into CH_2(^{3}B) + CO. Girard et al.[11] showed that the isomerization of HCCHO(^{3}A″) into the H_2CCO(^{3}A″) radical has a large barrier, which explains why the reaction proceeds favorably into HCCO + H as opposed to the CH_2 + CO channel. Both of the exit channels show a large translational energy release,[4] which suggests an exit channel barrier as indicated in the calculated overall profile of the potential energy surface in Figure 9a.

The Mechanism of the HCCO + O(^{3}P) Reaction. Calculations suggest[6] that there are several intermediate complexes that may form during the HCCO + O(^{3}P) reaction. However, the most stable intermediate, the OHCCO(^{2}A″) glyoxal radical, forms in a barrierless process, as indicated in Figure 9b. The decomposition of this intermediate has to cross only a small barrier (5 kcal/mol), which makes the lifetime of this intermediate comparatively short compared to the intermediates of the

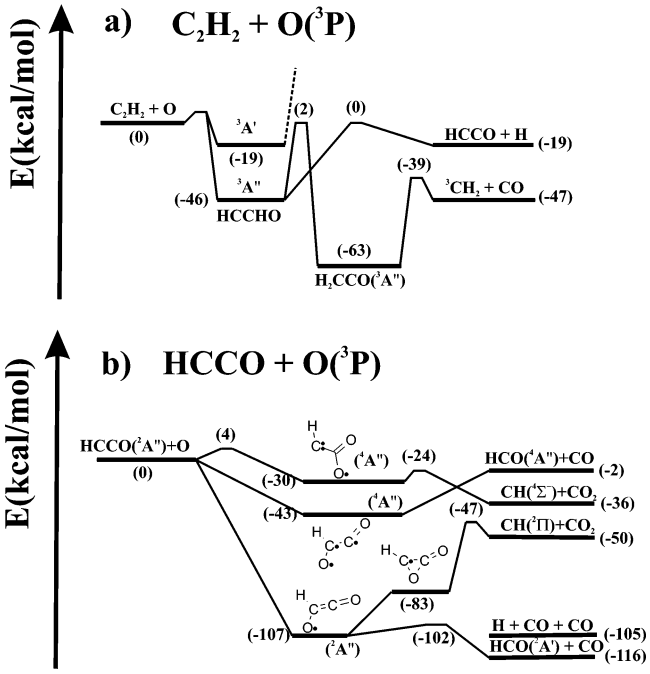

Figure 9. Schematic potential energy profiles for the (a) C_2H_2 + O(^{3}P)[12] and (b) HCCO + O(^{3}P)[6] reactions. The energies in brackets indicate the relative energies in kilocalories per mole (1 kcal/mol = 4.2 kJ/mol).

C_2H_2 + O(^{3}P) reaction. The available energy of the HCCO + O(^{3}P) is 102 kcal/mol, based on the exothermicity of the reaction. From the time-resolved results of the 193 nm photodissociation of ethyl ethynyl ether, 4.5 kcal/mol is channeled into the CO(v) vibrations, calculated with the vibrational fraction equation described in the previous section. The average fraction of energy that is channeled into the vibration is f_v = 0.043. From the linear combination of the Boltzmann populations, it is possible to separate the average fraction of the energy for both the cold (T_{vib}^1 = 2320 K) and hot (T_{vib}^2 = 10 300 K) parts of the bimodal distribution. From each vibrational temperature in Figure 7b for each process, the average fraction of energy for that process can be evaluated. The linear combination of these numbers should be equal to the previously determined value of f_v (0.043). The calculated values for the two parts of the distributions are f_{v1} = 0.022 (85%) and f_{v2} = 0.166 (15%), respectively. The relative fractions of the cold and hot distributions are shown in parentheses.

On the basis of the equipartition theorem, the average fraction of energy deposited to the CO vibration is f_{v1}^{stat} = 0.11 for the HCCO + O → HCO + CO process, which suggests that the hot part could arise from the first dissociation process. If the barrier energy (5 kcal/mol) indicated in Figure 9b was subtracted, the statistical value would be even lower compared to the experimental value (f_{v1} = 0.166), which suggests that the formation of the hot CO from the HCCO + O(^{3}P) reaction could originate in a more direct process. Recently, Peeters et al.[6] investigated the HCCO + O reaction system including the transition state of the glyoxal radical to form HCO + CO. Their results show that the C−C bond of this transition state is elongated and the CO bond is somewhat parallel to the C−C bond. Therefore, the dissociation of the HC(O)CO‡ could result in CO molecules with very large vibrational excitation but very little rotational excitation.

From equipartition, 63% of the total energy is available for HCO. The cold part of the observed distribution (f_{v2} = 0.022) is much smaller than the predicted statistical value (f_{v2}^{stat} = 0.12)

for $HCO \rightarrow H + CO$, which could be due to several reasons. Assigning a statistical distribution to the CO vibrations for the $HCO \rightarrow H + CO$ process is difficult, since the estimate of the available energy may be different than the 63% noted above. Also, the available energy for CO may be reduced due to the small binding energy (15 kcal/mol) of the CH bond in the HCO radical compared to the total available energy (110 kcal/mol). In addition, the HCO fragment contains a light H, which may carry away much of the energy in translation due to momentum conversation, resulting in the observed cold distribution.

Analysis of the relative contribution of the cold and hot parts of the vibrational distribution shows that the cold part is ~85% of the distribution, while the hot part is only 15%. On the basis of simple statistical considerations (numbers of CO product molecules), we would have expected that the cold part of the distribution should be more equal to the hot part of the distribution assuming that only one channel would lead to CO formation. This discrepancy suggests that another mechanism(s) could also take part in forming the final vibrational distribution of the HCCO + O reaction. There are two possible mechanisms. In previous sections, only the sequential dissociation process is considered, but there is a possibility of the concerted dissociation mechanism of the glyoxal radical, which may result in different distributions. Also, one of the possible reaction pathways is the formation of electronically excited HCO (see Figure 9b), which could also contribute to the final distribution of CO.

Acknowledgment. This work has been supported by the U.S. Department of Energy under the contract #DEAC03-76SF00098. The authors would like to thank the National Institute of Standards and Technology for the loan of some of the equipment used in this work.

References and Notes

(1) Brezinsky, K. *Prog. Energy Combust. Sci.* **1986**, *12*, 1.
(2) Westbrook, C. K.; Dryer, F. L. *Combust. Sci. Technol.* **1981**, *27*, 31.
(3) Michael, J. V.; Wagner, A. F. *J. Phys. Chem.* **1990**, *94*, 2453.
(4) Schmoltner, A. M.; Chu, P. M.; Lee, Y. T. *J. Chem. Phys.* **1989**, *91*, 5365.
(5) Peeters, J.; Schaekers, M.; Vinckier, C. *J. Phys. Chem.* **1986**, *90*, 6552.
(6) Peeters, J.; Langhans, I.; Boullart, W.; Nguyen, M. T.; Devriendt, K. *J. Phys. Chem.* **1994**, *98*, 11988.
(7) Baulch, D. L.; Cobos, C. J.; Cox, R. A.; Esser, C.; Frank, P.; Just, T.; Kerr, J. A.; Pilling, M. J.; Troe, J.; Walker, R. W.; Warnatz, J. *J. Phys. Chem. Ref. Data* **1992**, *21*, 411.
(8) Boullart, W.; Peeters, J. *J. Phys. Chem.* **1992**, *96*, 9810.
(9) Peeters, J.; Boullart, W.; Langhans, I. *Int. J. Chem. Kinet.* **1994**, *26*, 869.
(10) Peeters, J.; Vanhaelemeersch, S.; Vanhoeymissen, J.; Borms, R.; Vermeylen, D. *J. Phys. Chem.* **1989**, *93*, 3892.
(11) Girard, Y.; Chaquin, P. *J. Phys. Chem. A* **2003**, *107*, 10462.
(12) Harding, L. B.; Wagner, A. F. *J. Phys. Chem.* **1986**, *90*, 2974.
(13) Shaub, W. M.; Burks, T. L.; Lin, M. C. *Chem. Phys.* **1980**, *45*, 455.
(14) Vinckier, C.; Debruyn, W. *J. Phys. Chem.* **1979**, *83*, 2057.
(15) Williams, D. G. *J. Phys. Chem.* **1971**, *75*, 4053.
(16) Williams, D. G.; Bayes, K. D. *J. Phys. Chem.* **1969**, *73*, 1232.
(17) Capozza, G.; Segoloni, E.; Leonori, F.; Volpi, G. G.; Casavecchia, P. *J. Chem. Phys.* **2004**, *120*, 4557.
(18) Chikan, V.; Nizamov, B.; Leone, S. R. *J. Phys. Chem. A* **2004**, *108*, 10770.
(19) Krisch, M. J.; Miller, J. L.; Butler, L. J.; Su, H.; Bersohn, R.; Shu, J. *J. Chem. Phys.* **2003**, *119*, 176.
(20) Manatt, S. L.; Lane, A. L. *J. Quant. Spectrosc. Radiat. Transfer* **1993**, *50*, 267.
(21) Ahmed, S. M.; Kumar, V. *J. Quant. Spectrosc. Radiat. Transfer* **1992**, *47*, 359.
(22) Osborn, D. L. *J. Phys. Chem. A* **2003**, *107*, 3728.
(23) Unfried, K. G.; Curl, R. F. *J. Mol. Spectrosc.* **1991**, *150*, 86.
(24) Jacox, M. E.; Olson, W. B. *J. Chem. Phys.* **1987**, *86*, 3134.
(25) Baeva, M.; Luo, X.; Pfelzer, B.; Repsilber, T.; Uhlenbusch, J. *Plasma Sources Sci. Technol.* **2000**, *9*, 128.
(26) Carl, S. A.; Sun, Q.; Peeters, J. *J. Chem. Phys.* **2001**, *114*, 10332.
(27) Temps, F.; Wagner, H. G.; Wolf, M. *Z. Phys. Chem.* **1992**, *176*, 27.
(28) Murray, K. K.; Unfried, K. G.; Glass, G. P.; Curl, R. F. *Chem. Phys. Lett.* **1992**, *192*, 512.
(29) Yardley, J. T. *Introduction to Molecular Energy Transfer*; Academic Press: New York, 1980.
(30) Allen, D. C.; Simpson, C. *Chem. Phys.* **1980**, *45*, 203.
(31) Bauer, H. J.; Roesler, H. *Molecular Relaxation Processes*; Academic Press: New York, 1966.
(32) Wang, B. S.; Gu, Y. S.; Kong, F. N. *J. Phys. Chem. A* **1999**, *103*, 7395.
(33) Mantz, A. W.; Maillard, J. P.; Roh, W. B.; Rao, K. N. *J. Mol. Spectrosc.* **1975**, *57*, 155.
(34) Chandra, S.; Maheshwari, V. U.; Sharma, A. K. *Astron. Astrophys., Suppl. Ser.* **1996**, *117*, 557.
(35) Griffiths, P. R. *Fourier transform infrared spectrometry*, John Wiley: New York, 1986.
(36) Bohland, T.; Temps, F.; Wagner, H. G. *Ber. Bunsen-Ges. Phys. Chem.* **1984**, *88*, 1222.
(37) Reid, J. P.; Marcy, T. P.; Kuehn, S.; Leone, S. R. *J. Chem. Phys.* **2000**, *113*, 4572.
(38) Osborn, D. L.; Mordaunt, D. H.; Choi, H.; Bise, R. T.; Neumark, D. M.; Rohlfing, C. M. *J. Chem. Phys.* **1997**, *106*, 10087.
(39) Mordaunt, D. H.; Osborn, D. L.; Choi, H.; Bise, R. T.; Neumark, D. M. *J. Chem. Phys.* **1996**, *105*, 6078.
(40) Slagle, I. R.; Sarzynski, D.; Gutman, D.; Miller, J. A.; Melius, C. F. *J. Chem. Soc., Faraday Trans. 2* **1988**, *84*, 491.
(41) Hack, W.; Hoyermann, K.; Olzmann, M.; Zeuch, T. *Proc. Combust. Inst.* **2003**, *29*, 1247.
(42) Sheaffer, P. M.; Zittel, P. F. *J. Phys. Chem. A* **2000**, *104*, 10194.
(43) Burke, M. L.; Dimpfl, W. L.; Sheaffer, P. M.; Zittel, P. F.; Bernstein, L. S. *J. Phys. Chem.* **1996**, *100*, 138.